DECAY OF SUPERSONIC RECTANGULAR JET ISSUING FROM A NOZZLE WITH DIAGONAL EXPANSION RAMPS

***Surendra BOGADI*[*] *and B.T.N. SRIDHAR*[1]**

[*]Department of Aeronautical Engineering, Rajalakshmi Engineering College, Chennai, India.
[1]Department of Aerospace Engineering, Madras Institute of Technology, Anna University, India
*Corresponding author; E-mail: surendrabogadi@rajalakshmi.edu.in

This paper addresses the effect of diagonal placement of expansion ramps on the decay characteristics of a supersonic rectangular jet. The diagonal placements of ramps induce additional vortices near the nozzle exit apart from the corner vortices emanating from the rectangular corners which is further enhances jet decay. A Mach 1.8 rectangular jet issuing from a converging-diverging nozzle of aspect ratio 2 and Reynolds number 1.861×10^5 *is considered for the study. To avoid the losses in divergent section, the shape of cross-section from the throat was maintained rectangular. Numerical simulations and Schlieren image study were carried out to validate the experimental results obtained from total pressure data. Both experimental and numerical studies show that the expansion ramps played a significant role to enhance decay rate. The ramps placed on the minor side caused maximum supersonic core length reduction indicating accelerated decay. This minor side ramps were found to be more effective at over-expansion conditions whereas the major side ramps for under-expansion conditions. Also, both experimental and numerical studies have shown that shock waves are rendered weaker by the minor side placement of ramps at all expansion levels.*

Keywords: *rectangular jet, diagonal expansion ramps, supersonic core length, jet pressure decay, streamwise vortices, expansion waves, shock cell.*

1. Introduction

Understanding of supersonic jet mixing has been of substantial importance in the fields of high-speed aerospace combustion and jet exhaust noise suppression. Last three decades have seen many noteworthy findings in achieving faster decay of supersonic jets using rectangular nozzles.

Asymmetric nozzle shapes have been proposed by many researchers as effective means of passive control of supersonic jets. Mixing characteristics of jets issuing from rectangular nozzles were proved to be superior to those from circular nozzles. Krothapalli et al [1] and Gutmark et al [2] reported an increased spreading rate in rectangular nozzles caused by the streamwise vortical structures in the plane containing small dimension of underexpanded rectangular nozzles. The differences between circular and rectangular jets were noticed due mainly to the corner flow regions affecting the stability characteristics of the jet and its evolution. Axial vorticity mixing mechanism was proved to be effective in a supersonic flow environment by Tillman et al [3]. Supersonic core length was observed to be reduced by a factor of 2 for a supersonic jet from a rectangular nozzle than

that from a circular nozzle. Mohanta and Sridhar [4, 5] studied shock cell structures of supersonic asymmetric jets and found hydraulic diameter and major axis as major role players in dissipation rate.

In the past, various techniques have been explored to generate streamwise vortices and to improve mixing. Although the use of tabs is proved to be effective in enhancing mixing of supersonic jets, it results in thrust losses due to blockage effects of these vortex generators [6]. This motivated researchers to explore alternative techniques for generating streamwise vortices to enhance mixing [7-15]. Effects of nozzle trailing edge modifications on the flow structure and jet mixing with ambient air were explored by Kim and Samimy [7, 8]. Their results indicated that in non-ideally expanded flow regimes, pairs of streamwise vortices of various strength and sign were generated and the mixing was significantly enhanced. Sang et al [9] computationally studied mixing characteristics of underexpanded supersonic jets emerging from the plain and notched rectangular nozzles using nozzle exit boundary layer swirl as a mean of passive flow control. The mass flow rates in the jets were observed to be increased considerably, whereas the axial gross thrust penalty was minimal due to the induced boundary layer swirl. Gerlinger et al [10] studied the mixing enhancement of a Mach 2 model of scramjet combustor. They proposed lobbed strut geometry which created counter-rotating vortices. It was shown that the length to achieve a perfect mixing of hydrogen and air was strongly reduced by this technique. Northam [11, 12] and Davis et al [13] have conducted experiments on ramped injectors at supersonic Mach numbers and found that swept ramps yielded better mixing relative to the upswept ramps, by the generation of larger vortices with stronger axial vorticity. Similar results were obtained by the numerical study conducted by Drummand et al [14]. Donohue et al [15] found that the streamwise vortex generated by a ramp was stronger than that generated by baroclinic torque; i.e the source of the streamwise vorticity was proved to be a spanwise pressure gradient on the ramp.

The present study is a novel attempt to combine the merits of asymmetric jets [1-5] and trailing edge modifications [7-15]. Experimental and computational investigations were carried to study the effect of diagonally wall-mounted expansion ramps in accelerating the decay of an aspect ratio (AR) 2 rectangular supersonic jet. This diagonal arrangement of ramps is believed to create a strong spanwise pressure gradient resulting in the development of counter-rotating stream-wise vortices in the flow (Fig.1). This technique is expected to enhance jet mixing to a considerable level.

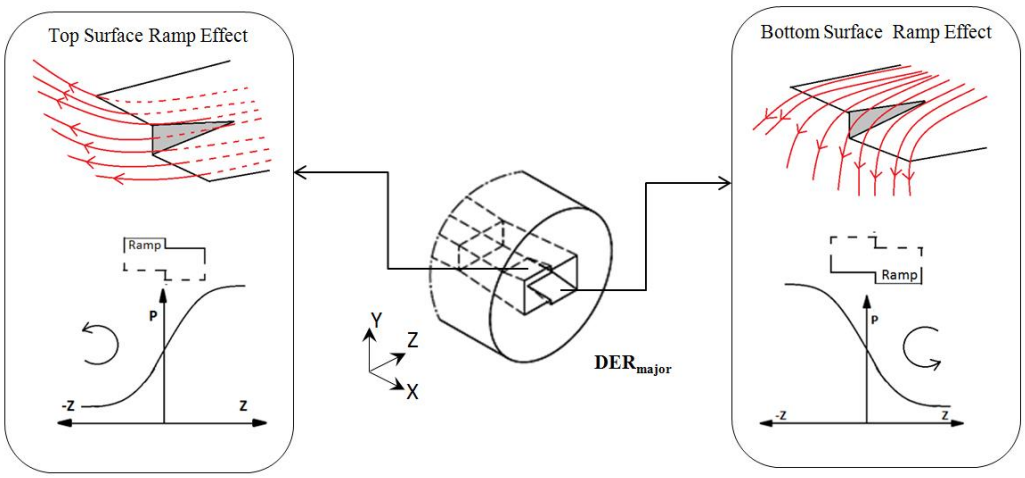

Figure 1. Anticipated pressure distributions, spanwise pressure gradients on the ramped wall of nozzles for the underexpanded case, and the resulting induced streamwise vortices

2. Experimental Model

The experimental models used in the present investigation are Mach 1.8 convergent-divergent rectangular nozzles of aspect ratio (AR) 2. The cross-section of the nozzles transforms from circular at the inlet to rectangular (AR2) at the throat, and to a larger rectangle (AR2) at the exit section maintaining the required area ratio (=exit area/throat area) of 1.44. Fig. 2 shows the dimensional details of plain rectangular nozzle model. The exit section views of ramped test nozzle models are given in Figs. 3(a) and 3(b). The ramps are fabricated on the diagonally opposing corners. The nozzles were fabricated using electrical discharge machining (EDM) technique. The equivalent diameters (=4*area/perimeter) at throat and exit sections of the plain rectangular nozzle are D^* =8.16 ± 0.01 mm and D_e = 9.8 ± 0.01 mm respectively.

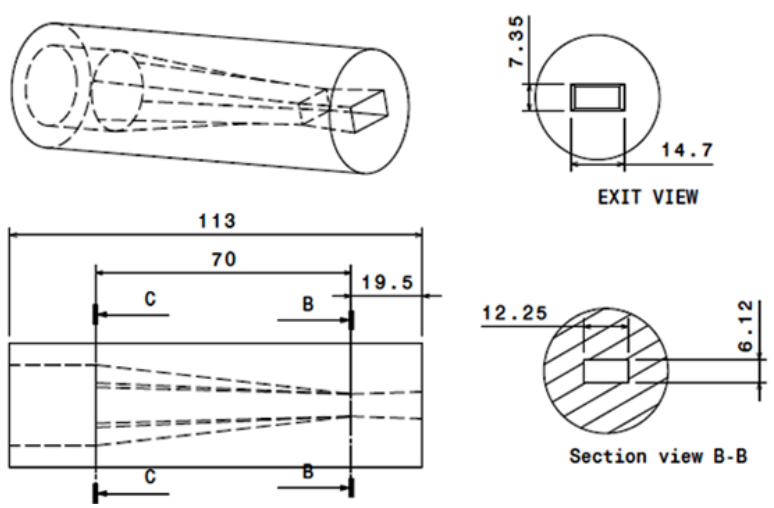

Figure 2. Dimensional details of plain rectangular nozzle test model (all dimensions are in mm)

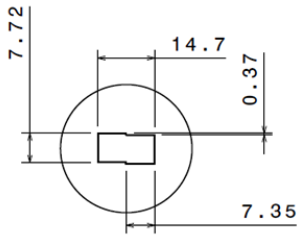

Figure 3(a). Diagonal ramps on the major side (DER*major*)

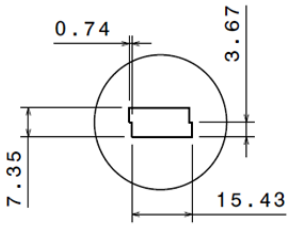

Figure 3(b). Diagonal ramps on the minor side (DER*minor*)

3. Experimental Details

The experiments were conducted in the free jet facility at the high-speed jet laboratory, Rajalakshmi Engineering College, Chennai, India. The facility consists of two heavy duty air compressors, air drier, reservoir, settling chamber, gate valves, pressure regulating valve (PRV), and pressure gauges (Fig. 4). Compressed air from the reservoir was ducted through a gate valve and a PRV to a settling chamber where it was brought to an equilibrium stagnation condition to reduce the flow disturbance caused by the PRV, a mitigation length of 1.5 m is provided between the PRV and the settling chamber. The flow was conditioned by two mesh screens placed within the settling chamber before entering into the nozzle. The inlet total pressure to the nozzle was achieved by controlling the settling chamber pressure (p_0) since the backpressure was the ambient pressure (p_a) into which the jet was discharged. Total pressures were measured with the help of a pitot probe connected to Net Scanner system 9116 (measuring precision of ± 0.05%) [16]. A robust 3-axis traverse mechanism available at the laboratory was automated using motion control boards, bipolar stepper motors of torque 25 kg-cm, timing belts and pulleys, potentiometer, DPDT switch, 24V Industrial power supply. This arrangement reduces uncertainty errors by enabled the pitot probe traverse linearly for recording pressure values at each 0.05 mm interval.

Figure 4. Free Jet Facility at High Speed Jet Laboratory of Rajalakshmi Engineering College

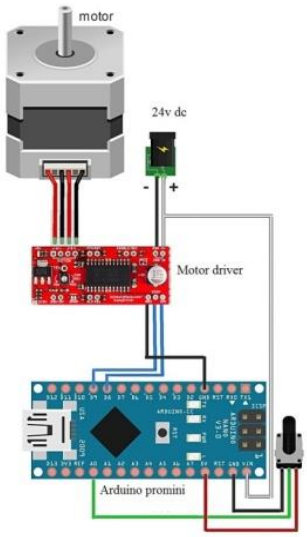

Figure 5. Traverse automation components

Fig. 5 shows the detailed arrangement of traverse automation components. A Z-type Schlieren setup was used for all flow visualization experiments. A 200 W halogen bulb was used as light source. The reflected beam from the second mirror was cut by a vertical knife. 20.1-megapixel CCD camera was used to capture the image at night shooting mode with exposure time (auto mode) 3-4 seconds.

4. Numerical Simulation

Numerical Simulations were carried out using ANSYS CFX solver. Domain and mesh sizes (Tab. 1) were finalized after performing numerical simulations for independency check. High mesh density regions were created in the areas of jet axis, near nozzle exit and in the entrainment zone. Prism layers were created on the nozzle inner surface to capture the wall shear layer effects. The domain and type of boundary conditions are shown in Fig. 6. The domain extends 8 D_e and 60 D_e in the radial and downstream directions respectively from the nozzle exit. For the present test conditions, this domain was tested for full development and recovery of the jet to atmospheric pressure. Reynolds Averaged Navier Stokes equations were solved for numerical solutions. The k-ω based SST model was considered for its ability to transport the turbulent shear stress and for highly accurate predictions of the onset and the amount of flow separation under adverse pressure gradients [18-20]. The convergence criterion for numerical computation is considered to be 10^{-4} for the RMS residual value.

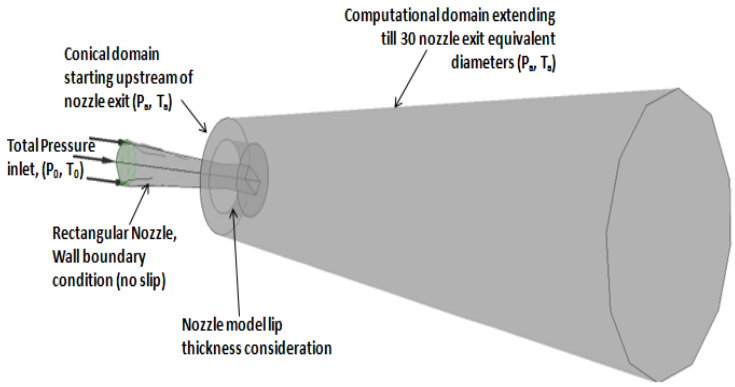

Figure 6. Domain and boundary conditions for numerical simulations

Table 1. Computational mesh statistics

Model	Nodes	Cells
Rectangular Nozzle	286520	1615341
DER_{major}	292118	1644969
DER_{minor}	292417	1645459

5. Results

Three main sources of streamwise vorticity in the supersonic jet with modified trailing edges are (i) the vorticity convected downstream in the boundary layer approaching the modified region; (ii) the spanwise pressure gradient on the nozzle inside surface; and (iii) the baroclinic torque due to the possible misalignment of pressure and density gradients [8]. The present study investigates the effect of diagonal expansion ramps introduced in the divergent portion extending up to converging-diverging (C-D) nozzle exit plane. Experimental and numerical results are presented in this section primarily focus on (i) identification of the effect of streamwise vortical structures, which governs jet development and evolution, on the mixing enhancement and (ii) shock cell development and progression in the supersonic core region. Tab. 2 shows the series of tests conducted in the present investigation. For the nozzle geometry considered, the absolute values of inlet total pressures 4, 6 and 8 bar represent over-expanded, slightly under-expanded and highly under-expanded jets respectively.

Table 2. List of experiments conducted (P_0 is absolute value of inlet total pressure in bar)

Test Model	Jet Pitot Pressures			Schlieren Visualization			CFX simulation		
	$p_0 = 4$	$p_0 = 6$	$p_0 = 8$	$p_0 = 4$	$p_0 = 6$	$p_0 = 8$	$p_0 = 4$	$p_0 = 6$	$p_0 = 8$
Rectangular Nozzle	✓	✓	✓	✓	✓	✓	✓	✓	✓
DER_{major}	✓	✓	✓	✓	✓	✓	✓	✓	✓
DER_{minor}	✓	✓	✓	✓	✓	✓	✓	✓	✓

5.1. Centerline Pitot Pressure Decay

Flow features of supersonic jet differ from those of subsonic jets. Potential core region doesn't exist in a supersonic jet because of the wave phenomena. The supersonic core length (L_{sc}) is defined as the axial distance up to which flow Mach number prevail to be supersonic. After this region, rapid decay of jet pitot pressure is caused by the viscous interactions. This region of rapid jet pressure decay is termed as characteristic decay zone and it lasts up to a certain axial extent. Followed by the characteristic decay region, the jet decays at a very low pace and gradually approaches zero velocity (close to ambient pressure) at a far downstream location. This region is called the fully developed zone.

A pitot probe placed in supersonic flow results in a bow shock formation ahead of the probe nose. This causes the probe to measure the pressures behind the bow shock (influenced by the probe) instead of true pressures (uninfluenced by the presence of probe). Also, the calculation of flow Mach numbers from these measured pitot pressures using the isentropic pressure–Mach number relation, the normal shock relation or the Rayleigh Pitot formula is inappropriate because of dominant wave phenomena [21]. The measured Pitot pressure (p_{0x}) along the jet axis (x-direction) has been nondimensionalized with the settling chamber pressure (p_0) and the dimensionless pressure (p_{0x}/p_0) has been plotted as a function of nondimensional axial distance (x/D_e). Jet centreline pressure decay indicates the mixing process with ambient fluid mass. Therefore, shorter decay length can be considered as an indication of efficient jet mixing. Because of wave domination in the jet core, pressure decay curves show oscillations in the near field. The end of the pressure oscillation indicates

the end of the core length of the supersonic jet. Thereafter the pressure decreases monotonically. The supersonic core length (L_{sc}) of the supersonic jet is also defined as the axial extent, from the nozzle exit, at which the characteristic decay begins [21].

After rapid centerline pressure decay in the characteristic zone, the jet becomes fully developed. In the fully developed region, the decay is gradual and therefore the centerline pressure curves in this region remain almost parallel to the x-axis. The centreline decay of the jet, for inlet total pressures 4, 6 and 8 bar, from the nozzles with diagonal expansion ramps on the major and minor sides is compared with that of the plain rectangular jet in Figs. 7-9. In comparison with plain rectangular jet, the diagonal expansion ramps on both major side (DER_{major}) and on the minor side (DER_{minor}) were found to accelerate jet mixing. As a result, the cores of the jets controlled with ramps are shorter than the uncontrolled (plain rectangular) jet core at all inlet total pressures of the present study. Also, the DER_{minor} jet has shown better decay than the DER_{major} jet.

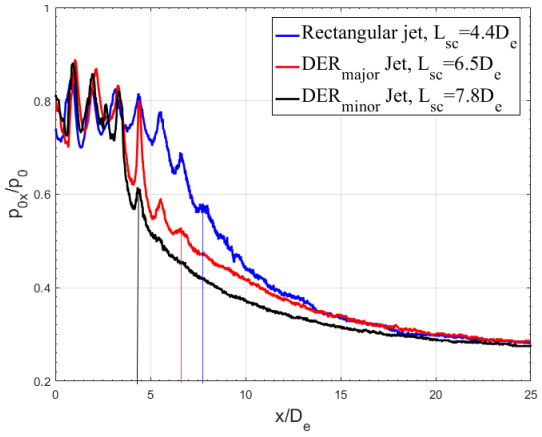

Figure 7. Jet axis pitot pressures at P_0 = 4 bar

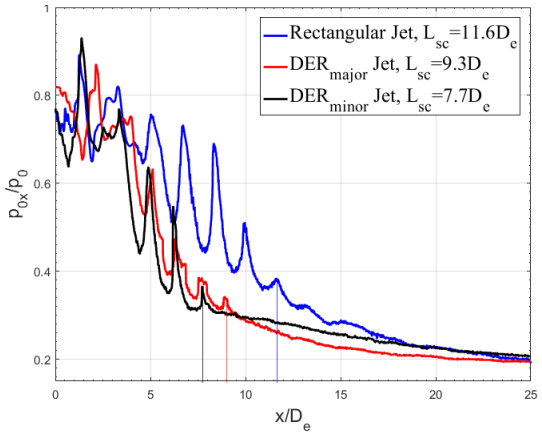

Figure 8. Jet axis pitot pressures at P_0 = 6 bar

For the Mach 1.8 jet (expanding into the free atmosphere), an inlet total pressure of 4 bar is an overexpanded condition. The jet experiences an adverse pressure gradient at the nozzle exit section. The pitot pressure decay plots of jets with and without expansion ramps at this expansion level are shown in Fig. 7. It is seen that both DER_{minor} and DER_{major} jets result in considerably lower levels of Pitot pressure in the core and characteristic decay regions. Lower pressure values indicate superior mixing of the jet caused by the DER_{minor} and DER_{major} jets. The decay of both DER_{minor} and DER_{major} jets is identical up to $x/D_e = 2.5$. Beyond $x/D_e = 2.5$ the DER_{minor} jet decays slightly faster. The core lengths (L_{sc}) for DER_{minor}, DER_{major}, and the plain rectangular jets are approximately $4.4D_e$, $6.5D_e$ and $7.8D_e$, respectively. This could also be due to the fact that a slight increment (5%) in the jet cross section because of the introduction of ramps.

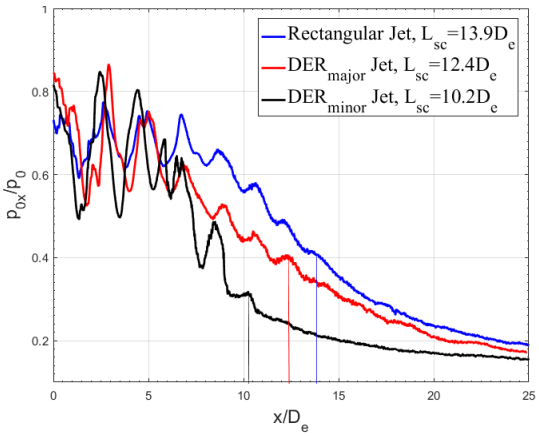

Figure 9. Jet axis pitot pressures at P_0 = 8 bar

The end of the pressure oscillation (or L_{sc}) for plain rectangular and ramped jets at $p_0 = 4$ bar is indicated by straight vertical lines in Fig. 7. The reduced Pitot pressure amplitude in the core region of the DER jets is an indication that the enhanced mixing caused by geometrically induced swirl weakens the waves in the jet core. Between DER$_{minor}$ and DER$_{major}$ geometries, DER$_{minor}$ found to be more efficient in weakening the waves.

The inlet total pressure $p_0 = 6$ bar indicates a marginally underexpanded jet. At this pressure also, the DER$_{minor}$ jet continue to perform better than the DER$_{major}$ jet, as shown by the pressure decay of DER$_{minor}$ jet in Fig. 8. It is observed that the mixing promotion of DER$_{minor}$ jet is superior to that of the DER$_{major}$ jet in the core and characteristic decay regions. Near-field mixing caused by the diagonal expansion ramps on the minor side reduces the core length from 11.6 D_e to 7.7 D_e. The core of the DER$_{major}$ jet is 17% greater than that of the DER$_{minor}$ jet. In the far-field (beyond 16 D_e), all jets show identical pressure decay.

The inlet total pressure $p_0 = 8$ bar indicates a highly underexpanded jet. In the presence of the negative pressure gradient also, the vortices shed from the corners of DER$_{minor}$ jet can efficiently promote mixing in the core region. As in the case of lower p_0 values, at $p_0 = 8$ bar the mixing of the DER$_{minor}$ jet is superior to that of the DER$_{major}$ jet, leading to a reduction in the core from 13.9 D_e to 10.2 D_e, whereas the DER$_{major}$ jet brings down the core only to 12.4 D_e. This is shown in Fig. 9.

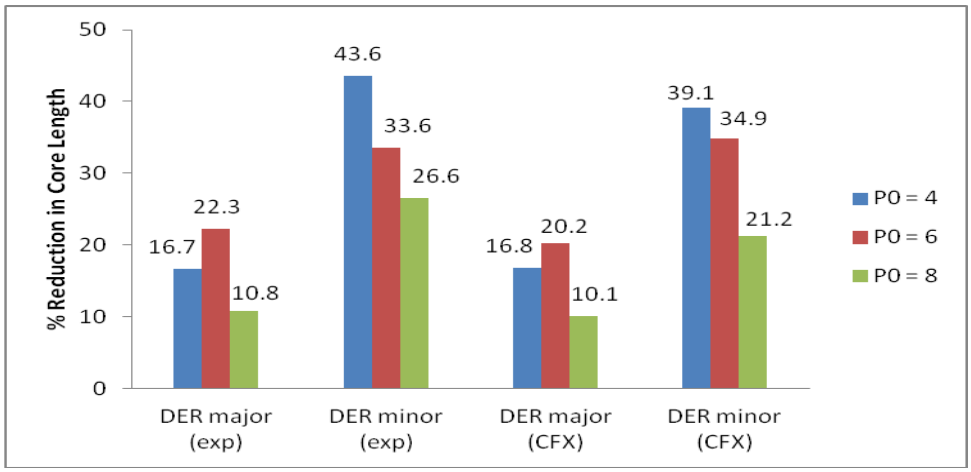

Figure 10. Comparison of core length reduction with respect to plain rectangular nozzle

From the centerline pressure decay results it is evident that in the presence of both adverse and favorable pressure gradients, the mixing promotion of DER$_{minor}$ jet is better than that of the DER$_{major}$ jet. The percentage changes in core length of these jets from both experimental and numerical results are shown in Fig. 10. From the pitot pressure fluctuations, the numbers of shock cells in the core are observed to be 7, 6 and 5 for Plain rectangular, DER$_{major}$ and DER$_{minor}$ jets respectively for all the inlet total pressures. The effectiveness of the diagonal expansion ramps is observed to be reduced with the increase in p_0.

6. Shock Visualization

Various authors have observed the length of a shock cell in different ways [22, 23]. In the context of the present study, a shock cell is considered to be the region which involves a complete cycle of waves that is one shock wave and one Prandtl-Meyer expansion fan. It is to be noted that the wave generated due to the reflection of the expansion waves is taken as another oblique shock wave.

Shock visualization study is performed using Schlieren imaging system and with the CFX Mach contours. Fig. 11 shows a comparison made of shock cells captured from Schlieren image and CFX Mach contour for DER_{minor} jet at $p_0 = 8$ bar. A close match has been found between the two methods with a maximum deviation of 3% (Tab. 3). Also, supersonic core lengths from numerical results of the plain rectangular jet were found to be in reasonable agreement with the empirical relation proposed by Mohanta and Sridhar [5].

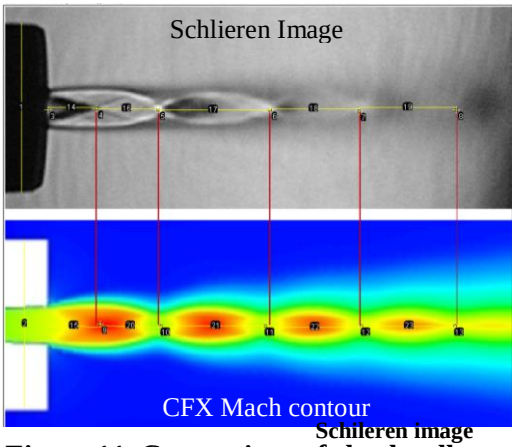

Figure 11. Comparison of shock cells obtained from Schlieren image and CFX Mach contour of DER_{minor} jet at $p_0 = 8$ bar

Table 3. Distances in terms of equivalent diameter for DER_{minor} jet at $p_0 = 8$ bar

location title	Experiment (Schlieren Visualization)	CFX (Mach contour)
Nozzle outer diameter	3.47	3.47
Expansion wave reflection location from the nozzle exit	0.94	0.97
First shock cell length (Regular Reflection)	2.23	2.30
Second shock cell length	2.25	2.19
Third shock cell length	1.85	1.85
Fourth shock cell length	1.95	1.94

Figs. 12 - 14 show the Schlieren images of the near field jet structures in nozzle minor and major axes planes for plain rectangular DER_{major} and DER_{minor} jets respectively. Figs. 15-17 show the shock cells captured from numerical simulations for all test cases. The following observations were made from both Schlieren and numerical images.

Comparison of Schlieren images captured in the major and minor axis planes of plain rectangular jet clearly depict the asymmetric, three-dimensional nature of shock wave system. The images of DER_{major} and DER_{minor} (Figs. 13 & 14) show multiple reflections from the nozzle exit in addition to the ones observed from the plain rectangular jet. These additional expansion waves are originating from the expansion ramps and reflecting further into the jet core. The shear layers consist of both supersonic and subsonic regions in the direction normal to the jet axis. The turbulent mixing taking place in the jet shear layer reduces the strength and spacing of these shock cells in the downstream direction. This is proved with the measured shock cell lengths for first four shock cells (Tab. 3). From Fig. 14, it is seen that the ramps on the minor side cause thicker shear layer at all inlet total pressures and faster weakening of the waves in the core region. This is because of the stronger vortices created by the larger ramp angles of DER_{minor} model in comparison with DER_{major} model.

Highly underexpanded symmetric jets exhibit Mach reflection in the first shock cell region [22]. In contrast, in the present study, regular symmetric reflections were observed for both overexpanded and underexpanded jets in the first shock cell (Figs. 13c & 14c). This can be justified with two reasons. (i) A comparatively weak pressure gradient and flow turning caused by the nozzle inlet total pressures [23]. (ii) Weaker wave strength in the core of non-circular supersonic jets. Therefore, this absence of Mach reflections is a direct indication of weakened shock strength and enhanced mixing of the underexpanded controlled jets. The location of regular reflections moves far from the nozzle exit plane and the length of shock cells increase with the increase in p_0.

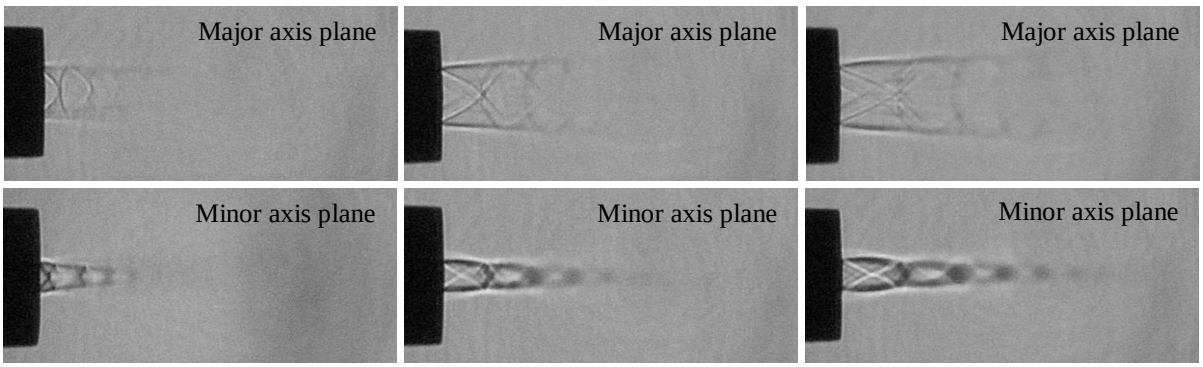

(a) P_0 = 4 bar **(b) P_0 = 6 bar** **(c) P_0 = 8 bar**

Figure 12. Schlieren images of plain rectangular jet

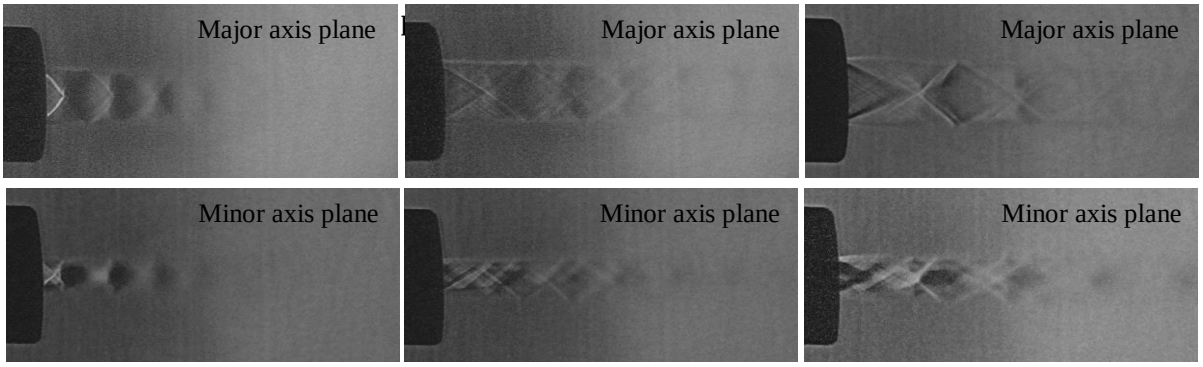

(a) P_0 = 4 bar **(b) P_0 = 6 bar** **(c) P_0 = 8 bar**

Figure 13. Schlieren images of DER_{major} Jet

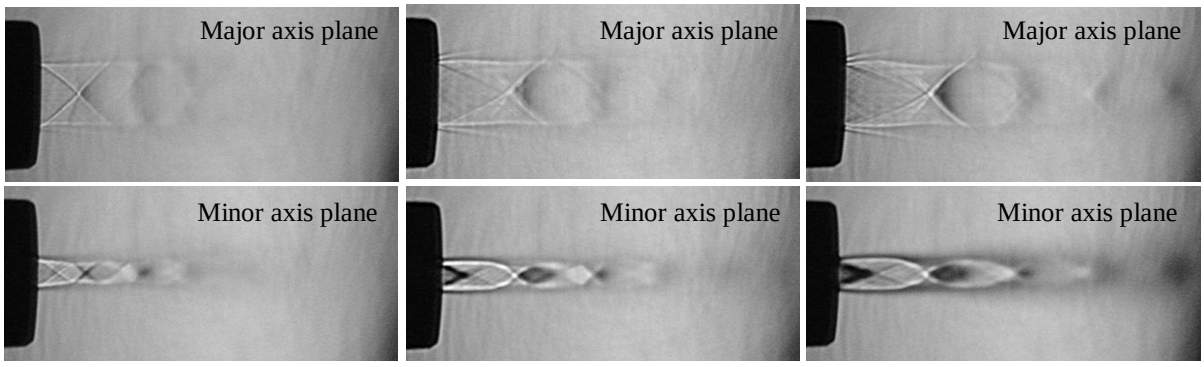

(a) P_0 = 4 bar **(b) P_0 = 6 bar** **(c) P_0 = 8 bar**

Figure 14. Schlieren images of DER_{minor} Jet

The mixing area for the under expanded results (from Mach contours presented in Figs 15-17) is observed to be substantially larger than other test conditions at all axial locations. The relatively smaller mixing of overexpanded baseline rectangular nozzle (Fig. 15) can be attributed to the inward directing flows caused by compression waves which restrict outward development of jet. The number of shock cells for all test pressures were observed to be 7, 6 and 5 for plain rectangular, DER_{major} and DER_{minor} jets respectively (Figs 15-17).

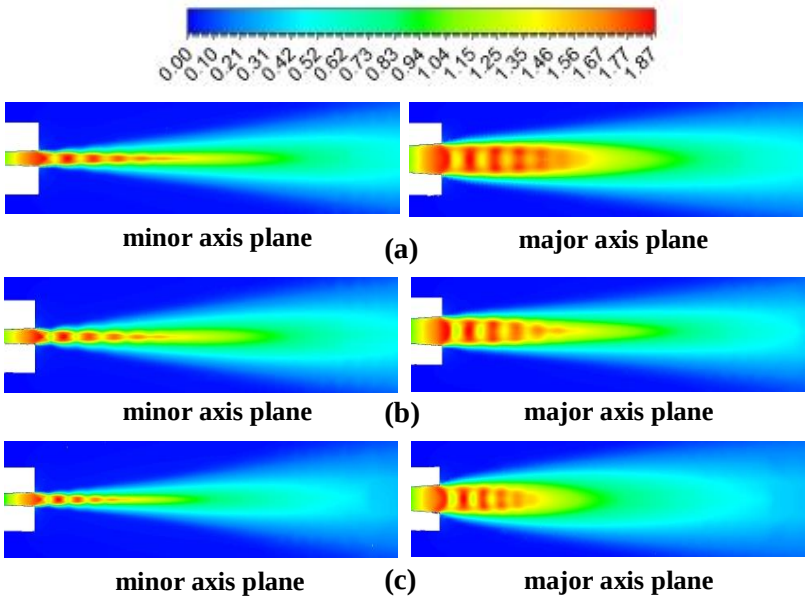

Figure 15.
Mach contours at $p_0 = 4$ bar
(a) Plain Rectangular Jet
(b) DER_{major} Jet and
(c) DER_{minor} Jet

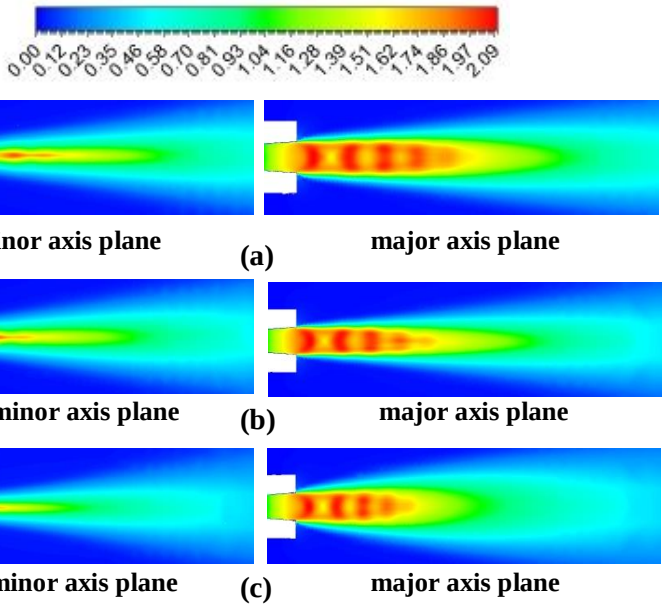

Figure 16.
Mach contours at $p_0 = 6$ bar
(a) Plain Rectangular Jet
(b) DER_{major} Jet and
(c) DER_{minor} Jet

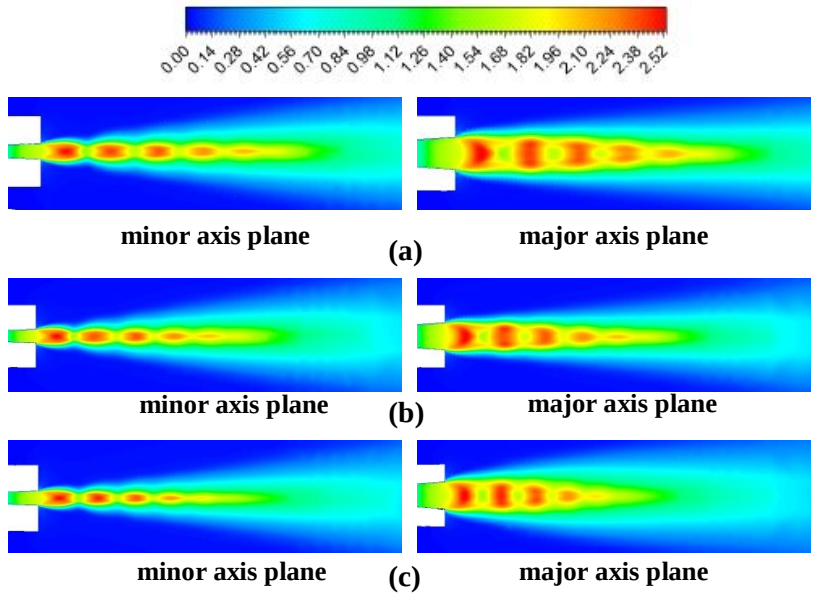

Figure 17.
Mach contours at $p_0 = 8$ bar
(a) Plain Rectangular Jet
(b) DER_{major} Jet and
(c) DER_{minor} Jet

7. Conclusion

The present study indicates expansion ramps as mixing promoters. A more detailed spreading behavior study is needed to prove the same. Furthermore, the present experimental and numerical results show that expansion ramps on the minor side of a C-D rectangular nozzle are more effective in mixing promotion than that of the expansion ramps on the major side at all inlet total pressures at Mach 1.8 and Reynolds number 1.861×10^5. Of all test cases studied, the enhanced near-field mixing caused by the ramps on the minor side results in core length reduction and weaker waves in the jet core. This is due to the strong induced vortex caused on minor side. The DER_{minor} cause a maximum core length reduction of 44% at p_0 = 4 bar and a minimum of 27% at p_0 = 8 bar. The maximum and minimum core length reductions caused by the ramps placed on the major side are 22% and 11% at inlet total pressures 6 and 8 bar respectively. The waves present in the jet core for DER_{minor} are found to be weaker than those for DER_{major} of the same area ratio. The Schlieren images confirm the thick shearing of jets caused by the ramps on the minor side. In addition, the Schlieren images show that the waves in the core of the jet for DER_{minor} are considerably weaker than the waves in the core of the plain rectangular jet. A more detailed spreading behavior study is needed to prove the same.

Acknowledgment

The financial support provided by University Grants Commission, India (No.F MRP 6150/15, SERO/UGC) is gratefully acknowledged.

Nomenclature

AR	Ratio of lengths of major side to minor side of the rectangular cross section.
D_e	equivalent diameter of the exit section of rectangular nozzle, [m]
DER_{major}	nozzle with expansion ramps cut at the diagonal opposites on the major length side of exit section
DER_{minor}	nozzle with expansion ramps cut at the diagonal opposites on the minor length side of exit section
L_{sc}	Supersonic core length
p_0	nozzle inlet total pressure (absolute), [Nm^{-2}]
p_a	ambient pressure (absolute), [Nm^{-2}]
p_{0x}	pitot pressure along the jet centerline axis, [Nm^{-2}]
X, Y, Z	Cartesian coordinates fixed along the the jet axis (centerline of the jet), minor and major axis of the nozzle exit plane respectively.
x	distance along the jet centerline, starting from nozzle exit [m]

References

[1] Krothapalli A., *et al.*, The role of screech tones on the mixing of an underexpanded rectangular jet, *J. of Sound and Vibration.*, *106* (1986), 1, pp. 119-143

[2] Gutmark E, *et al.*, Near Acoustic Field and Shock Structure of Rectangular Supersonic Jet, *AIAA, 28* (1990), 7, pp. 1164-1170

[3] Tillman T. G., *et al.*, Enhanced mixing of supersonic jets, *Journal of Propulsion and Power, 7* (1991), 6, pp.1006-1014
[4] Mohanta P. K., Sridhar B. T. N., Study of Decay Characteristics of Hexagonal and Square Supersonic Jet, *Int. J. Turbo Jet Engines, 34* (2016), 2, DOI: https://doi.org/10.1515/tjj-2016-0001
[5] Mohanta P. K., Sridhar B. T. N., Study of decay characteristics of rectangular and elliptical supersonic jets, *Thermal Science, 21* (2017), 6B, pp. 3001-3010
[6] Ahuja K. K., Brown W. H., Shear flow control by mechanical tabs, *AIAA 2nd Shear Flow Conference*, No. 89-0994, 1989.
[7] Samimy M. *et al.*, Passive Control of Supersonic Rectangular Jets via Nozzle Trailing-Edge Modifications, *AIAA, 36* (1998), 7, pp. 1230-1239
[8] Kim J. H., Samimy M., Mixing enhancement via nozzle trailing edge modifications in a high-speed rectangular jet, Physics of Fluids, *11* (1999), 9, pp. 2731-2742
[9] Sang Y. H., Passive control of supersonic rectangular jets through boundary layer swirl, *Int. J. Turbo* Jet-Engines, 30 (2013), 2, pp. 199-216
[10] Gerlinger P., *et al.*, Numerical Investigation of mixing and combustion enhancement in supersonic combustors by strut induced streamwise vorticity, *Aerospace Science and Technology, 12* (2008), 2, pp. 159-168
[11] Northam G. B., Evaluation of Parallel Injector Configurations for Supersonic Combustion, *25th Joint Propulsion Conference, AIAA-89-2525*, 1989
[12] Northam G. B., *et al.*, Mach 2 and Mach 3 Mixing and Combustion in Scramjets, *27th Joint Propulsion Conference, AIAA-91-2394*, 1991
[13] Davis D. O., Hingst W. R., Progress Toward Synergistic Hypermixing Nozzles, *27th Joint Propulsion Conference, AIAA-91-2264*, 1991.
[14] Drummond J. P., *et al.*, Mixing Enhancement in a Supersonic Combustor, 25th *Joint Propulsion Conference, AIAA-89-2794*, 1989
[15] Donohue J. M., *et al.*, Vorticity Generation Mechanisms in Parallel Injection Schemes for Supersonic Mixing, *28th Joint Propulsion Conference, AIAA-92-3286*, 1992
[16] http://www.te.com/usa-en/product-CAT-SCS0002.html?source=header-match#mdp-tabs-content
[17] Miller R. S., *et al.*, Numerical simulation of non-circular jets, *Computers & Fluids, 24* (1995), 1, pp. l-25.
[18] Sarkar S., Lakshmanan B., Application of a Reynolds Stress Turbulence Model to the Compressible Shear Layer, *AIAA, 29* (1991), 5, pp. 743-749
[19] Menter F. R., Two-equation eddy-viscosity turbulence models for engineering applications, *AIAA, 32* (1994), 8, pp. 1598- 1605
[20] Bardina J. E., *et al.*, Turbulence Modeling Validation Testing and Development, *NASA Technical report 110446*, 1997
[21] Rathakrishnan E., *Applied gas dynamics*, Wiley P. New Jersey 2010: pp. 485-563
[22] Mehta R. C., Prasad J. K., Estimation of the shock-cell structure of an axisymmetric supersonic free jet, *Indian J. of Engineering and Material Sciences, 13* (1996), pp. 141-147
[23] Arun Kumar R., Rajesh G., Shock transformation and hysteresis in underexpanded confined jets, *J. Fluid Mech., 823* (2017), pp. 538-561